Science
AAAS

The Chemical Structure of a Molecule Resolved by Atomic Force Microscopy

Leo Gross, *et al.*

Science **325**, 1110 (2009);
DOI: 10.1126/science.1176210

The following resources related to this article are available online at www.sciencemag.org (this information is current as of September 10, 2009):

Updated information and services, including high-resolution figures, can be found in the online version of this article at:
http://www.sciencemag.org/cgi/content/full/325/5944/1110

Supporting Online Material can be found at:
http://www.sciencemag.org/cgi/content/full/325/5944/1110/DC1

This article **cites 25 articles**, 4 of which can be accessed for free:
http://www.sciencemag.org/cgi/content/full/325/5944/1110#otherarticles

This article appears in the following **subject collections**:
Chemistry
http://www.sciencemag.org/cgi/collection/chemistry

Information about obtaining **reprints** of this article or about obtaining **permission to reproduce this article** in whole or in part can be found at:
http://www.sciencemag.org/about/permissions.dtl

Downloaded from www.sciencemag.org on September 10, 2009

Science (print ISSN 0036-8075; online ISSN 1095-9203) is published weekly, except the last week in December, by the American Association for the Advancement of Science, 1200 New York Avenue NW, Washington, DC 20005. Copyright 2009 by the American Association for the Advancement of Science; all rights reserved. The title *Science* is a registered trademark of AAAS.

only appears when looking at the I_{mix} signal, its high Q is only an effective quality factor, but it is useful for applications that, for instance, rely on precise measurements of the resonance frequency (*21*).

These results show that the coupling between the mechanics and the electron transport can be very strong in SWNTs. In comparison, experiments on microfabricated semiconductor resonators, which are coupled to metal single-electron transistors, have not shown any oscillations of f_0 and Q (*22*). This difference probably arises from the much greater mass of these resonators as compared with those of SWNTs, so that they are much less sensitive to the motion of individual tunneling electrons. A way to quantify the coupling is by looking at the damping rate caused by the interaction between the mechanics and the electron transport, $\gamma_{e-ph} = 2\pi f_0/Q$. Damping rate can be useful for the evaluation of quantum electromechanics phenomena in analogy to laser cooling of, for example, trapped ions (*23*). We have γ_{e-ph} as high as 3×10^6 Hz for nanotubes, which compares with $\gamma_{e-ph} \sim 0.7$ Hz for macroscopic atomic force microscopy cantilevers (*24*). As for single-electron transistors that are superconducting, γ_{e-ph} is expected to be enhanced (*15*). In this case, however, γ_{e-ph} measured on microfabricated resonators is below 5×10^4 Hz (*12*).

The strong coupling in nanotubes holds promise for various applications. We have shown that it allows for a widely tunable nonlinearity of the resonator dynamic. Nonlinearity of the motion is useful for sensitivity improvement of mass and force sensing (*25*), mechanical signal amplification (*26*, *27*), noise squeezing (*28*), study of quantum behaviors of macroscopic systems (*29*), mechanical microwave computing (*30*), or energy harvesting via vibration-to-electricity conversion (*31*). We emphasize that the nonlinearity in nanotubes can be tuned by an electronic means (by changing V_g^{DC}), which is convenient for practical use. In comparison, the nonlinearity in previously studied nanoresonators comes from purely mechanical effects (which can be described by the Duffing equation). There, the nonlinearity can be modified by using strain, but this is complicated to do experimentally. The strong coupling in nanotubes could also be used for cooling mechanical oscillations to the ground state (*32*), which would open the possibility to study nonclassical states at a mesoscopic scale. The ability to electrically tune the coupling (with V_g^{DC}) would then be very useful for quantum manipulation.

References and Notes

1. V. Sazonova *et al.*, *Nature* **431**, 284 (2004).
2. P. Poncharal, Z. L. Wang, D. Ugarte, W. A. Heer, *Science* **283**, 1513 (1999).
3. B. Reulet *et al.*, *Phys. Rev. Lett.* **85**, 2829 (2000).
4. S. T. Purcell, P. Vincent, C. Journet, V. T. Binh, *Phys. Rev. Lett.* **89**, 276103 (2002).
5. B. Witkamp, M. Poot, H. S. J. van der Zant, *Nano Lett.* **6**, 2904 (2006).
6. D. Garcia-Sanchez *et al.*, *Phys. Rev. Lett.* **99**, 085501 (2007).
7. B. Lassagne, D. Garcia-Sanchez, A. Aguasca, A. Bachtold, *Nano Lett.* **8**, 3735 (2008).
8. K. Jensen, K. Kim, A. Zettl, *Nat. Nanotechnol.* **3**, 533 (2008).
9. H.-Y. Chiu, P. Hung, H. W. C. Postma, M. Bockrath, *Nano Lett.* **8**, 4342 (2008).
10. A. Eriksson *et al.*, *Nano Lett.* **8**, 1224 (2008).
11. J.-C. Charlier, X. Blase, S. Roche, *Rev. Mod. Phys.* **79**, 677 (2007).
12. A. Naik *et al.*, *Nature* **443**, 193 (2006).
13. Materials and methods are available as supporting material on *Science* Online.
14. M. Brink, thesis, Cornell University (2007).
15. A. A. Clerk, S. Bennett, *N. J. Phys.* **7**, 238 (2005).
16. We took $C_{dot} = 57$ aF from Fig. 2A. Dissipation caused by He gas used to thermalize the resonator was included by calculating the total quality factor as $(\sum 1/Q_i)^{-1}$. The contribution of Q from He has been measured to be 1035 by means of pumping the gas, which left the temperature stable for a short moment.
17. We obtained $C_g'^2/k = 6 \times 10^{-22}$ F^2/Nm, which has to be compared with $C_g' \approx 10^{-13}$–10^{-12} F/m obtained by using commercial simulators and $k \approx 10^{-4}$–10^{-3} N/m from (*1*). The value of Γ is 3×10^9 s^{-1}, which is somewhat smaller than expected in the quantum regime $\Gamma = 8k_BTG_{max}/e^2 \approx 9 \times 10^{10}$ s^{-1} (where G_{max} is the maximum conductance of a Coulomb-blockade peak). In addition, the shape of the measured oscillations of f_0 and Q differs to some extent from what is predicted (Fig. 3). These differences may arise from the fact that the nanotube dot is not perfect (the Coulomb blockade peaks are not fully periodic in V_g^{DC}, and the peak heights are different). Another explanation is that the model that was used is too simple to quantitatively capture the physics (*33*, *34*).
18. The oscillation of Q as a function of V_g^{DC} has been observed in a second device. The Coulomb-blockade oscillations of G are, however, less regular than the ones presented here, and so the nanotube probably consists of a series of quantum dots (*35*).
19. W. G. Conley, A. Raman, C. M. Krousgrill, S. Mohammadi, *Nano Lett.* **8**, 1590 (2008).
20. L. D. Landau, E. M. Lifshitz, *Mechanics* (Pergamon Press, Oxford, 1960).
21. When V_g^{AC} is low, the values of f_0 and Q extracted from $I_{mix}(f)$ are the same as the ones from $\delta z(f)$.
22. R. G. Knobel, A. N. Cleland, *Nature* **424**, 291 (2003).
23. C. Raab *et al.*, *Phys. Rev. Lett.* **85**, 538 (2000).
24. M. T. Woodside, P. L. McEuen, *Science* **296**, 1098 (2002).
25. J. S. Aldridge, A. N. Cleland, *Phys. Rev. Lett.* **94**, 156403 (2005).
26. A. Erbe *et al.*, *Appl. Phys. Lett.* **77**, 3102 (2000).
27. R. L. Badzey, P. Mohanty, *Nature* **437**, 995 (2005).
28. R. Almog, S. Zaitsev, O. Shtempluck, E. Buks, *Phys. Rev. Lett.* **98**, 078103 (2007).
29. V. Peano, M. Thorwart, *Phys. Rev. B* **70**, 235401 (2004).
30. S. B. Shim, M. Imboden, P. Mohanty, *Science* **316**, 95 (2007).
31. F. Cottone, H. Vocca, L. Gammaitoni, *Phys. Rev. Lett.* **102**, 080601 (2009).
32. S. Zippilli, G. Morigi, A. Bachtold, *Phys. Rev. Lett.* **102**, 096804 (2009).
33. A. D. Armour, M. P. Blencowe, Y. Zhang, *Phys. Rev. B* **69**, 125313 (2004).
34. F. Pistolesi, S. Labarthe, *Phys. Rev. B* **76**, 165317 (2007).
35. B. Gao, D. C. Glattli, B. Placais, A. Bachtold, *Phys. Rev. B* **74**, 085410 (2006).

36. We thank G. Morigi and J. Moser for discussions. The research has been supported by the European Union–funded projects FP6-IST-021285-2 and FP6-ICT-028158, and the Swedish Foundation for Strategic Research.

Supporting Online Material

www.sciencemag.org/cgi/content/full/1174290/DC1
Materials and Methods

31 March 2009; accepted 19 June 2009
Published online 23 July 2009;
10.1126/science.1174290
Include this information when citing this paper.

Downloaded from www.sciencemag.org on September 10, 2009

The Chemical Structure of a Molecule Resolved by Atomic Force Microscopy

Leo Gross,[1]* Fabian Mohn,[1] Nikolaj Moll,[1] Peter Liljeroth,[1,2] Gerhard Meyer[1]

Resolving individual atoms has always been the ultimate goal of surface microscopy. The scanning tunneling microscope images atomic-scale features on surfaces, but resolving single atoms within an adsorbed molecule remains a great challenge because the tunneling current is primarily sensitive to the local electron density of states close to the Fermi level. We demonstrate imaging of molecules with unprecedented atomic resolution by probing the short-range chemical forces with use of noncontact atomic force microscopy. The key step is functionalizing the microscope's tip apex with suitable, atomically well-defined terminations, such as CO molecules. Our experimental findings are corroborated by ab initio density functional theory calculations. Comparison with theory shows that Pauli repulsion is the source of the atomic resolution, whereas van der Waals and electrostatic forces only add a diffuse attractive background.

Noncontact atomic force microscopy (NC-AFM), usually operated in frequency-modulation mode (*1*), has become an important tool in the characterization of nanostructures on the atomic scale. Recently, impressive progress has been made, including atomic resolution with chemical identification (*2*) and measurement of the magnetic exchange force with atomic resolution (*3*). Moreover, lateral (*4*) and vertical (*5*) manipulation of atoms and the determination of the vertical and lateral forces during such manipulations (*6*) have been demonstrated. Striking results have also been obtained in AFM investigations of single molecules. For example, atomic resolution was achieved on single-walled carbon nanotubes (SWNTs) (*7*, *8*), and the force needed to switch a molecular conformation was measured (*9*).

However, the complete chemical structure of an individual molecule has so far not been imaged with atomic resolution. The reasons that make AFM investigations on single molecules so challenging are the strong influence of the exact

[1]IBM Research, Zurich Research Laboratory, 8803 Rüschlikon, Switzerland. [2]Debye Institute for Nanomaterials Science, Utrecht University, Post Office Box 80000, 3508 TA Utrecht, Netherlands.

*To whom correspondence should be addressed. E-mail: lgr@zurich.ibm.com

atomic composition and the geometry of the tip, as well as the relatively low stability of the system, which can result in unintentional lateral or vertical manipulation of the molecule during imaging. As will be shown below, both problems can be solved by preparing a well-defined tip by deliberately picking up different atoms and molecules with the tip apex. The exact knowledge of the tip termination also facilitates quantitative comparison with first-principles calculations, which is essential for understanding the nature of the tip-sample interaction.

To benchmark AFM resolution on molecules, we investigated pentacene ($C_{22}H_{14}$, Fig. 1A), a well-studied linear polycyclic hydrocarbon consisting of five fused benzene rings. State-of-the-art scanning tunneling microscopy (STM) studies of pentacene on metal, such as Cu(111) (*10*), and thin-film insulators, such as NaCl on Cu(111) (*11*, *12*), have been performed recently. On insulating films, STM was used to image the molecular orbitals near the Fermi level, E_F, whereas on metals the molecular orbitals were broadened and distorted because of coupling to the electronic states of the substrate. STM is sensitive to the density of states near E_F, which extends over the entire molecule. This prevents the direct imaging of the atomic positions (or core electrons) in such planar aromatic molecules by STM. In this work, we present atomically resolved AFM measurements of pentacene both on a Cu(111) substrate and on a NaCl insulating film.

For atomic resolution with the AFM, it is necessary to operate in the short-range regime of forces, where chemical interactions give substantial contributions. In this force regime, it is desirable to work with a cantilever of high stiffness with oscillation amplitudes on the order of 1 Å, as pointed out by Giessibl (*13*). Our low-temperature STM/AFM has its basis in a qPlus sensor design (*14*) and is operated in an ultrahigh vacuum at a temperature of 5 K. The high stiffness of the tuning fork [spring constant $k_0 \approx 1.8 \times 10^3$ N/m (*15*), resonance frequency f_0 = 23,165 Hz, and quality factor $Q \approx 5 \times 10^4$] allows stable operation at oscillation amplitudes down to 0.2 Å. A metal tip (*16*) was mounted on the free prong of the tuning fork, and a separate tip wire (which is insulated from the electrodes of the tuning fork) was attached to measure the tunneling current (*17*). The bias voltage V was applied to the sample.

Modification of the STM tip apex is known to have a profound influence on the achievable image resolution (*10*, *11*, *18*, *19*). We explored the effects of controlled atomic-scale modification of the AFM tip and show that suitable tip termination results in dramatically enhanced atomic scale contrast in NC-AFM imaging. We imaged pentacene molecules (Fig. 1A) in STM (Fig. 1B) and AFM (Fig. 1, C and D) modes on Cu(111) by using a CO-terminated tip. For these measurements, a CO molecule was deliberately picked up with the tip (*16*), which led to an increased resolution in the AFM mode (see below). From previous investigations, it is known that the CO molecule is adsorbed with the carbon atom toward the metal tip (*18*, *19*).

The CO molecule slightly affects the STM image, and several faint maxima and minima are visible because of the interaction of the CO with the pentacene orbitals, similar to the effect of a pentacene-modified tip (*10*). The AFM images (Fig. 1, C and D) were recorded in constant-height mode; that is, the tip was scanned without z feedback parallel to the surface while the frequency shift Δf was being recorded (*16*). In this and all of the following measurements, the tip height z is always given with respect to the STM set point over the substrate. The use of constant-height operation was critical because it allowed stable imaging in the region where Δf is a nonmonotonic function of z. In the AFM images (Fig. 1, C and D), the five hexagonal carbon rings of each pentacene molecule are clearly resolved. We observed local maxima of $\Delta f(x, y)$ above the edges of the hexagons, near the carbon atom positions, and minima above the centers of the carbon rings (hollow sites), in concordance to the measurements on SWNTs (*7*). Even the carbon-hydrogen bonds are imaged, indicating the positions of the hydrogen atoms within the pentacene molecule. Additionally, each molecule is surrounded by a dark halo.

To demonstrate that imaging conditions are also stable for the case of organic molecules on insulators, we used a thin insulating layer [NaCl(2 ML)/Cu(111), that is, two atomic layers of NaCl on Cu(111)] as substrate (Fig. 2). Furthermore, to study the influence of the tip termination, we performed measurements with different atomic modifications of the tip apex. In addition to the Ag- (Fig. 2A) and CO-terminated (Fig. 2B) tips, we also recorded Δf images with

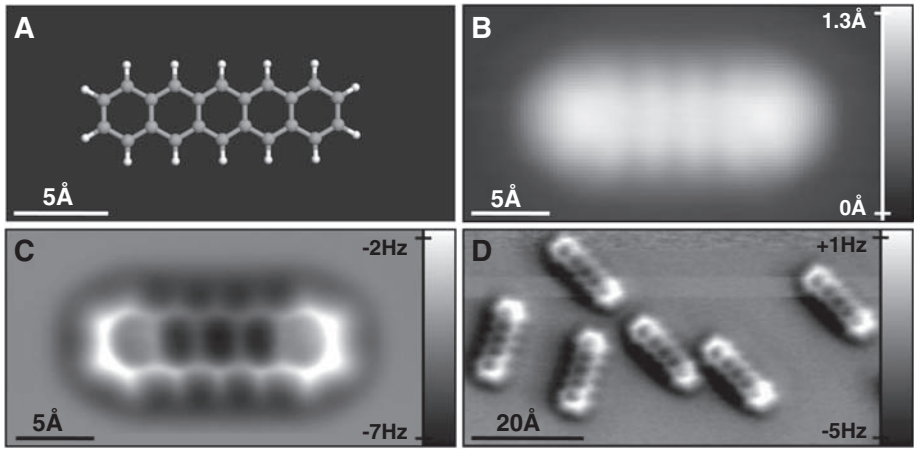

Fig. 1. STM and AFM imaging of pentacene on Cu(111). (**A**) Ball-and-stick model of the pentacene molecule. (**B**) Constant-current STM and (**C** and **D**) constant-height AFM images of pentacene acquired with a CO-modified tip. Imaging parameters are as follows: (B) set point I = 110 pA, V = 170 mV; (C) tip height z = –0.1 Å [with respect to the STM set point above Cu(111)], oscillation amplitude A = 0.2 Å; and (D) z = 0.0 Å, A = 0.8 Å. The asymmetry in the molecular imaging in (D) (showing a "shadow" only on the left side of the molecules) is probably caused by asymmetric adsorption geometry of the CO molecule at the tip apex.

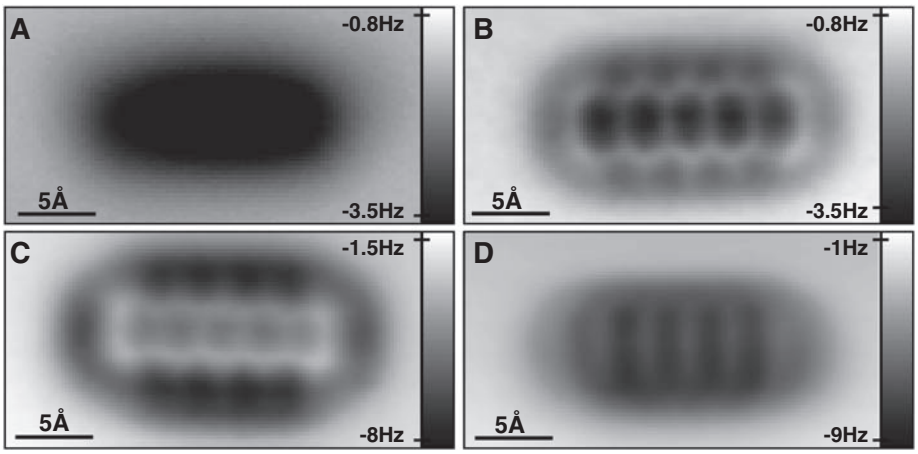

Fig. 2. Constant-height AFM images of pentacene on NaCl(2ML)/Cu(111) using different tip modifications (*16*). (**A**) Ag tip, z = –0.7 Å, A = 0.6 Å; (**B**) CO tip, z = +1.3 Å, A = 0.7 Å; (**C**) Cl tip, z = –1.0 Å, A = 0.7 Å; and (**D**) pentacene tip, z = +0.6 Å, A = 0.5 Å. The z values are given with respect to a STM set point of I = 2 pA, V = 200 mV above the NaCl(2 ML)/Cu(111) substrate.

Downloaded from www.sciencemag.org on September 10, 2009

tips modified with Cl (Fig. 2C) and pentacene (Fig. 2D) (*16*). For each tip, the tip height z was minimized; that is, decreasing z further by a few 0.1 Å resulted in unstable imaging conditions, usually leading to the molecule being laterally displaced or picked up by the tip. Comparing the different tips, we see that their atomic termination is crucial for the contrast observed above the molecule. The highest lateral resolution was observed with CO-modified tips, and the contrast above pentacene is similar to that in the measurements on Cu(111). With metal-terminated tips

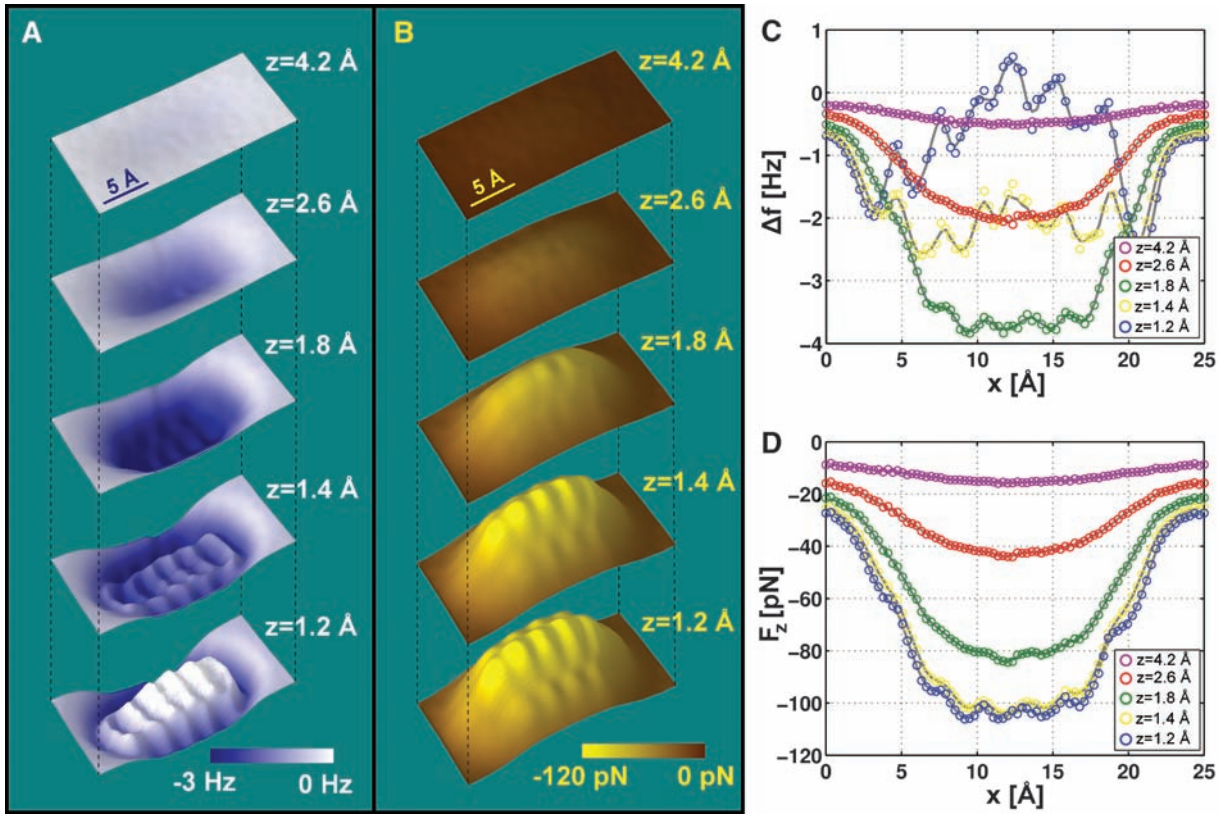

Fig. 3. Maps of measured frequency shift Δf (**A**) and extracted vertical force F_z (**B**) at different tip heights z. Corresponding line profiles of Δf (**C**) and F_z (**D**) along the long molecular axis. The data shown are part of a complete three-dimensional force field that has been measured in a box of 25 Å by 12.5 Å by 13 Å above a pentacene molecule (*16*). The z values are given with respect to a STM set point of I = 2 pA, V = 200 mV above the NaCl(2 ML)/Cu(111) substrate.

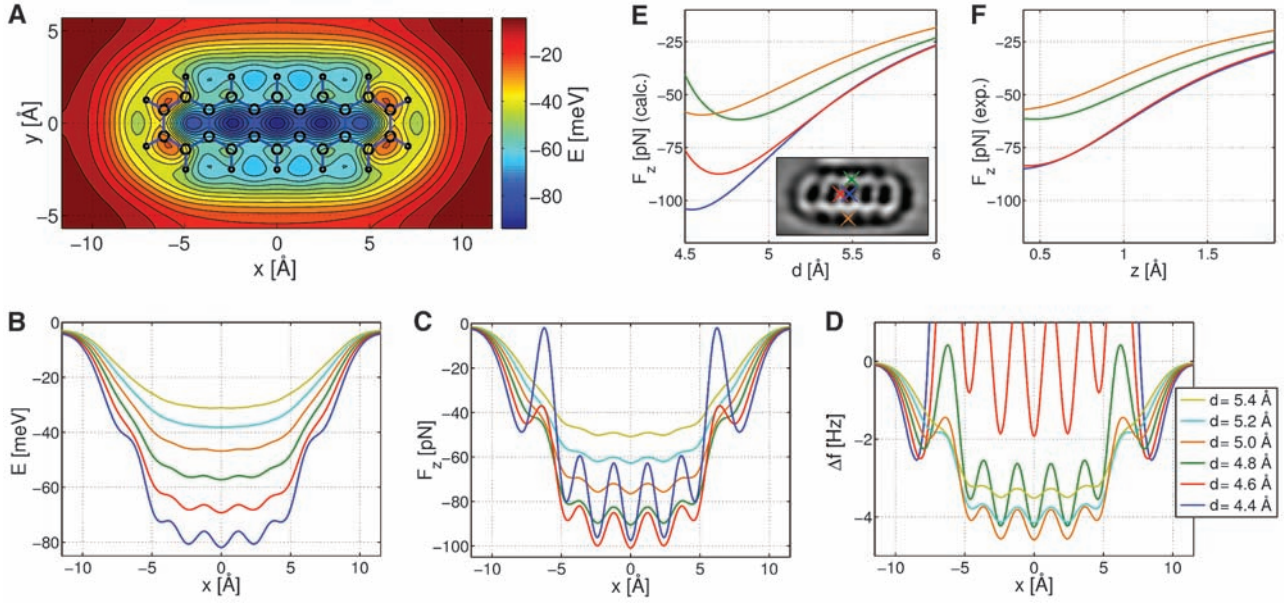

Fig. 4. Calculated energy map (**A**) for a CO-pentacene distance of d = 4.5 Å. Calculated line profiles of the energy (**B**), the vertical force (**C**), and Δf (**D**) above the long molecular axis for different molecular distances. Calculated (**E**) and measured (**F**) force-distance curves above different molecular sites: central hollow site (blue), C-C bond of central ring on long molecular axis (red), C atom of central ring on short molecular axis (green), and H atom on short axis (orange). The inset in (E) shows a measured Δf map with the different molecular sites indicated. In the experimental data, the force components that arise from the metal tip behind the CO molecule have been subtracted (*16*, *29*).

Downloaded from www.sciencemag.org on September 10, 2009

(Ag, Au, or Cu), the molecule would always be manipulated (usually being picked up by the tip from NaCl) before the minimum of $\Delta f(z)$ was reached, and no atomic resolution could be observed in AFM measurements. The Cl termination yielded a contrast similar to that of the CO tip. However, in the AFM image acquired with the Cl tip, the minima above the hollow sites are less pronounced and the carbon rings appear smaller in diameter compared with the CO-terminated tip. The pentacene-modified tip gave a completely different contrast compared with all the other tips investigated, which indicates the strong influence of the tip modification.

In the following, we concentrate on the investigation of pentacene on NaCl(2 ML)/Cu(111) with a CO-terminated tip. We describe how the contrast depends on the tip sample distance, quantify the forces acting on the tip, and lastly compare the measurements to density functional theory (DFT) calculations in order to separate the contributions of different forces and understand the origin of the observed contrast. Frequency shift and force versus distance relations were determined by capturing a three-dimensional (x, y, z) field (*16*, *20*, *21*) of the frequency shift with 80 by 40 by 3100 data points in a box of 25 Å by 12.5 Å by 13 Å above a pentacene molecule. We extracted the vertical forces $F_z(x, y, z)$ with use of the method of Sader and Jarvis (*16*, *22*). Figure 3A shows the measured frequency shift at different tip heights, and the extracted vertical force is shown in Fig. 3B. Corresponding line profiles along the long molecular axis are given in Fig. 3, C and D, for Δf and F_z, respectively.

For distances greater than z = 4.2 Å (top image in Fig. 3A), we recorded only relatively small long-range forces (F_z < 20 pN), and the molecule was imaged as a featureless depression (attractive interaction). With decreasing tip height, $\Delta f(z)$ decreased before reaching a minimum (of about –4 Hz) above the molecular center at $z \approx 1.8$ Å. Near the minimum of $\Delta f(z)$, we started observing corrugation on the atomic scale (Fig. 3C). When we decreased z further, Δf increased again and finally became even positive over some parts of the molecule at z = 1.2 Å. The lateral contrast of Δf generally increased with decreasing tip height (Fig. 3C). At the height at which Δf crossed zero ($z \approx 1.2$ Å), we achieved the highest contrast and lateral resolution with AFM. This is the regime of maximal attractive forces (*16*). Decreasing the tip height further would result in instabilities and lastly in picking up the molecule by the tip.

In the force maps (Fig. 3B), we likewise observed how the contrast increased with decreasing z. For the smallest accessible tip height, that is, z = 1.2 Å, we measured an attractive force of 110 pN above the central carbon ring. Above the positions of the carbon atoms, the absolute values of the forces were smaller (between 60 and 90 pN) (*15*). These values are comparable to the maximum short-range forces acting on a silicon tip above the hollow sites and the carbon positions of a SWNT, which were recently measured as 106 pN and 75 pN, respectively (*7*) (also with a systematic error of about 30%).

To further elucidate the origin of the observed atomic contrast, we carried out DFT calculations (*16*, *23*, *24*) with highly optimized plane-wave code CPMD (*25*). We applied the PBE (Perdew-Burke-Ernzerhof) exchange-correlation functional (*26*) and used ab initio norm-conserving pseudopotentials (*27*). Van der Waals (vdW) forces were added semiempirically to the dispersion energy as a contribution proportional to R^{-6} (where R is the atomic distance) (*28*). We only included the pentacene molecule and the CO molecule in our calculations and neglected both the substrate and the metallic part of the tip. We assumed for the calculations that the CO molecule is perpendicular to the plane of the pentacene molecule, with the oxygen atom pointing toward the pentacene (*16*).

The calculated interaction energy surface is given in Fig. 4A, and the calculated constant-height line profiles of the energy, the vertical force, and Δf along the central molecular axis are shown in Fig. 4, B, C, and D, respectively. The intermolecular distance d denotes the distance of the CO carbon atom to the plane of the pentacene atoms. Experiment and theory (compare Figs. 3D and 4C) concordantly showed maximal attractive forces on the order of 100 pN above the hollow sites of the pentacene molecule, whereas attractive forces above the C-C bonds were smaller. The difference in the forces measured above these two sites increased with decreasing tip height. In the short-range regime (d < 5 Å), differences between calculations and experiment can be observed. In the calculations, sharp peaks appear above the outer C-C bonds (x = 6.4 Å and x = –6.4 Å in Fig. 4, C and D), which are less pronounced in the measurements (Fig. 3, C and D).

For a comparison between theory and experiment, we have to estimate the contribution of the metallic tip behind the CO molecule that was not included in the calculations. For this purpose, we measured the force acting on a purely metallic tip, then picked up a CO molecule and measured the force again under otherwise identical conditions. The difference of the forces for identical tip positions yielded the estimated contribution from the CO molecule only. We observed that the CO contribution to the force predominates in the relevant regime, whereas the metallic part of the tip contributed only about 30% to the attractive forces and gave no corrugation on the atomic scale (*16*). Calculated force-versus-distance curves (Fig. 4E) above different molecular sites around the central carbon ring of the molecule are compared with experimental data, with the contribution of the metallic tip subtracted (Fig. 4F). We observe good qualitative agreement between theory and experiment in terms of the maximal values of the force and the relative order in which the maximal attractive forces are reached above the different atomic sites (*29*). Quantitatively, the agreement is excellent for d > 5 Å. In the short-range regime (4.5 Å < d < 5 Å), the calculations overestimate the difference in the forces above the C-C bond and the hollow site. These discrepancies in the short-range region might arise because of the simplifications assumed in the calculations, namely not taking the substrate or the tip behind the CO into account and the semiempirical treatment of vdW forces. Another origin of the discrepancies could be the increasing influence of noise in the experimental data for small z values.

The calculations take into account forces of three different physical origins, namely electrostatic forces, vdW forces, and Pauli repulsive forces. Comparing their contributions to the overall force, we found that the electrostatic forces are small (~10%) compared with the vdW forces. These two contributions to the force show little lateral corrugation on the atomic scale and yield a diffuse attractive potential above the entire molecule, giving rise to the observed dark halo surrounding the molecules in the Δf maps. The origin of the atomic contrast is the Pauli repulsion force, which becomes substantial when regions of high electron density overlap. These regions are concentrated to the atomic positions and to the C-C (and to a lesser extent also to the C-H) bonds in the pentacene molecule and are revealed for sufficiently small tip-sample distances ($d \approx 5$ Å).

We conclude that atomic resolution in NC-AFM imaging on molecules can only be achieved by entering the regime of repulsive forces because the vdW and electrostatic forces only contribute a diffuse attractive background with no atomic-scale contrast. Modifying the tip with suitable atomic or molecular terminations is required to allow the AFM to be operated in this regime while maintaining stable imaging conditions. The tip termination governs the AFM contrast, and exact knowledge of the tip is needed for a detailed interpretation of the force measurements. In the case of the CO-terminated tip, we observed a spectacular enhancement of the atomic-scale contrast and were able to resolve the atomic positions and bonds inside pentacene molecules, precisely revealing the atomic molecular structure. It may also be possible to extract details about intermolecular bonds, for example, bond order and length. Furthermore, we foresee probing the reactivity of different molecular sites with respect to the known molecule or atom at the tip apex. Such investigations could yield detailed insight into chemical reactions and catalysis. Lastly, a combination of NC-AFM with electrostatic force microscopy could be used to investigate single-electron transport and charge distributions in metal-molecule systems on the atomic scale.

References and Notes

1. T. Albrecht, P. Grütter, D. Horne, D. Rugar, *J. Appl. Phys.* **69**, 668 (1991).
2. Y. Sugimoto *et al.*, *Nature* **446**, 64 (2007).
3. U. Kaiser, A. Schwarz, R. Wiesendanger, *Nature* **446**, 522 (2007).

Downloaded from www.sciencemag.org on September 10, 2009

4. Y. Sugimoto *et al.*, *Nat. Mater.* **4**, 156 (2005).
5. Y. Sugimoto *et al.*, *Science* **322**, 413 (2008).
6. M. Ternes, C. P. Lutz, C. F. Hirjibehedin, F. J. Giessibl, A. J. Heinrich, *Science* **319**, 1066 (2008).
7. M. Ashino, A. Schwarz, T. Behnke, R. Wiesendanger, *Phys. Rev. Lett.* **93**, 136101 (2004).
8. M. Ashino *et al.*, *Nat. Nanotechnol.* **3**, 337 (2008).
9. Ch. Loppacher *et al.*, *Phys. Rev. Lett.* **90**, 066107 (2003).
10. J. Lagoute, K. Kanisawa, S. Fölsch, *Phys. Rev. B* **70**, 245415 (2004).
11. J. Repp, G. Meyer, S. M. Stojkovic, A. Gourdon, C. Joachim, *Phys. Rev. Lett.* **94**, 026803 (2005).
12. J. Repp, G. Meyer, S. Paavilainen, F. E. Olsson, M. Persson, *Science* **312**, 1196 (2006).
13. F. J. Giessibl, *Rev. Mod. Phys.* **75**, 949 (2003).
14. F. J. Giessibl, *Appl. Phys. Lett.* **76**, 1470 (2000).
15. Mainly because of the uncertainty in the spring constant of the cantilever, a systematic error of 30% is estimated for the measured forces.
16. Materials and methods are available as supporting material on *Science* Online.
17. M. Heyde, M. Sterrer, H.-P. Rust, H.-J. Freund, *Appl. Phys. Lett.* **87**, 083104 (2005).
18. L. Bartels *et al.*, *Phys. Rev. Lett.* **80**, 2004 (1998).
19. H. J. Lee, W. Ho, *Science* **286**, 1719 (1999).
20. H. Hölscher, S. M. Langkat, A. Schwarz, R. Wiesendanger, *Appl. Phys. Lett.* **81**, 4428 (2002).
21. B. J. Albers *et al.*, *Nat. Nanotechnol.* **4**, 307 (2009).
22. J. E. Sader, S. P. Jarvis, *Appl. Phys. Lett.* **84**, 1801 (2004).
23. P. Hohenberg, W. Kohn, *Phys. Rev.* **136**, B864 (1964).
24. W. Kohn, L. J. Sham, *Phys. Rev.* **140**, A1133 (1965).
25. CPMD, IBM Corporation and MPI für Festkörperforschung Stuttgart, www.cpmd.org/.
26. J. P. Perdew, K. Burke, M. Ernzerhof, *Phys. Rev. Lett.* **77**, 3865 (1996).
27. D. R. Hamann, *Phys. Rev. B* **40**, 2980 (1989).
28. S. Grimme, *J. Comput. Chem.* **27**, 1787 (2006).
29. The experimental and theoretical distance values z and d could be related to each other, for example, by comparing the position of the force minimum above a certain molecular site. However, the experimental z position of the force minimum varies significantly between measurements with different CO tips (in Fig. 3 the force minimum was already reached at $z \approx 1.2$ Å, whereas in Fig. 4F it is not reached until $z \approx 0.4$ Å). We attribute this to the fact that the tunneling current, and hence the tip height corresponding to the STM set point, strongly depends on the exact adsorption geometry of the CO molecule at the tip apex. Therefore, we abstain from giving an explicit relation between z and d.
30. We thank A. Curioni, J. Repp, and R. Allenspach for valuable discussions and comments and M. Heyde and F. J. Giessibl for fruitful discussions on instrumental issues. The research leading to these results has received funding from the Swiss National Center of Competence in Research (NCCR) "Nanoscale Science" and from the European Community's Seventh Framework Programme under grant agreement no. 214954 (HERODOT). P.L. gratefully acknowledges funding by the Nederlandse Organisatie voor Wetenschappelijk Onderzoek (Chemical Sciences, Vidi-grant 700.56.423).

Supporting Online Material
www.sciencemag.org/cgi/content/full/325/5944/1110/DC1
Materials and Methods
Figs. S1 to S5
References

12 May 2009; accepted 2 July 2009
10.1126/science.1176210

Downloaded from www.sciencemag.org on September 10, 2009

Amplifying the Pacific Climate System Response to a Small 11-Year Solar Cycle Forcing

Gerald A. Meehl,[1]* Julie M. Arblaster,[1,2] Katja Matthes,[3,4] Fabrizio Sassi,[5] Harry van Loon[1,6]

One of the mysteries regarding Earth's climate system response to variations in solar output is how the relatively small fluctuations of the 11-year solar cycle can produce the magnitude of the observed climate signals in the tropical Pacific associated with such solar variability. Two mechanisms, the top-down stratospheric response of ozone to fluctuations of shortwave solar forcing and the bottom-up coupled ocean-atmosphere surface response, are included in versions of three global climate models, with either mechanism acting alone or both acting together. We show that the two mechanisms act together to enhance the climatological off-equatorial tropical precipitation maxima in the Pacific, lower the eastern equatorial Pacific sea surface temperatures during peaks in the 11-year solar cycle, and reduce low-latitude clouds to amplify the solar forcing at the surface.

It has long been noted that the 11-year cycle of solar forcing is associated with various phenomena in Earth's climate system, in both the troposphere and stratosphere (*1*–*9*). Because the amplitude of the solar cycle (solar maximum to solar minimum) is relatively small, about 0.2 W m^{-2} globally averaged (*10*), and the observed global sea surface temperature (SST) response of about 0.1°C would require more than 0.5 W m^{-2} (*11*), there has always been a question regarding how this small solar signal could be amplified to produce a measurable response.

Postulated mechanisms that could amplify the relatively small solar forcing signal to produce such responses in the troposphere include changes in clouds in the troposphere caused by galactic cosmic rays, or associated global atmospheric electric circuit variations, though neither has been plausibly simulated in a climate model. However, there are two other plausible mechanisms, though each has not yet produced a modeled response of the magnitude seen in the observations. The first involves a "top down" response of stratospheric ozone to the ultraviolet (UV) part of the solar spectrum that varies by a few percent. Peaks in solar forcing cause the enhanced UV radiation, which stimulates additional stratospheric ozone production and UV absorption, thus warming that layer differentially with respect to latitude. The anomalous temperature gradients provide a positive feedback through wave motions to amplify the original solar forcing. The changes in the stratosphere modify tropical tropospheric circulation and thus contribute to an enhancement and poleward expansion of the tropical precipitation maxima (*5*, *12*–*16*). The first demonstration of the top-down mechanism in a modeling study showed a broadening of the Hadley cells in response to enhanced UV that increased as the solar-induced ozone change was included (*17*).

A second "bottom up" mechanism that can magnify the response to an initially small solar forcing involves air-sea coupling and interaction with incoming solar radiation at the surface in the relatively cloud-free areas of the subtropics. Thus, peaks in solar forcing produce greater energy input to the ocean surface in these areas, evaporating more moisture, and that moisture is carried by the trade winds to the convergence zones where more precipitation occurs. This intensified precipitation strengthens the Hadley and Walker circulations in the troposphere, with an associated increase in trade wind strength that produces greater equatorial ocean upwelling and lower equatorial SSTs in the eastern Pacific, a signal that was first discovered in observational data (*1*, *2*). The enhanced subsidence produces fewer clouds in the equatorial eastern Pacific and the expanded subtropical regions that allow even more solar radiation to reach the surface to produce a positive feedback (*18*, *19*). Dynamical air-sea coupling produces a transition to higher eastern equatorial SSTs a couple of years later (*20*, *21*). There is observational evidence for a strengthened Hadley circulation in peak solar forcing years associated with intensified tropical precipitation maxima, a stronger descending branch in the subtropics, and a stronger ascending branch in the lower latitudes (*3*); a poleward expansion of the Hadley circulation in peak solar years, with stronger ascending motions at the edge of the rising branch, as well as a stronger Walker circulation with enhanced upward motions in the tropical western Pacific connected to stronger descending motions in the tropical eastern Pacific (*7*); and enhanced summer season off-equatorial climatological monsoon precipitation over India (*6*, *22*). This cold event–like response to peak solar forcing is different from cold events (also known as La Niña events)

[1]National Center for Atmospheric Research, Post Office Box 3000 Boulder, CO 80307, USA. [2]Center for Australian Weather and Climate, Bureau of Meteorology, Melbourne, Australia. [3]Helmholtz Centre Potsdam – GFZ German Research Centre for Geosciences, Potsdam, Germany. [4]Institut für Meteorologie, Freie Universität Berlin, Berlin, Germany. [5]Naval Research Laboratory, Washington, DC 20375, USA. [6]Colorado Research Associates, Boulder, CO 80301, USA.

*To whom correspondence should be addressed. E-mail: meehl@ncar.ucar.edu